The Journal of Supercritical Fluids 216 (2025) 106442

Contents lists available at ScienceDirect

The Journal of Supercritical Fluids

journal homepage: www.elsevier.com/locate/supflu

Dye removal from wastewater using nanostructured chitosan aerogels produced by supercritical CO_2 drying

Alessandra Zanotti, Lucia Baldino, Stefano Cardea *, Ernesto Reverchon

Department of Industrial Engineering, University of Salerno, Via Giovanni Paolo II, 132, Fisciano, SA 84084, Italy

HIGHLIGHTS

- Chitosan aerogels were produced using supercritical CO_2 drying at 200 bar/35 °C.
- 50 mg of 3 % w/w nanostructured chitosan aerogels were used for dye adsorption.
- Crystal Violet removal was enhanced with respect to Methyl Orange.
- The system dye-aerogel behaves differently at low and large driving forces.
- Both dyes follow Freundlich isotherm and a pseudo-second order kinetics.

GRAPHICAL ABSTRACT

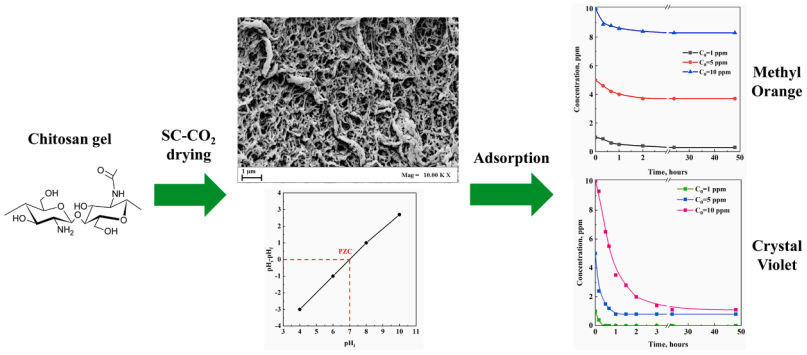

ARTICLE INFO

Keywords:
Aerogel
Chitosan
Supercritical drying
Dyes
Adsorption kinetics

ABSTRACT

Background: Dyes abundance in wastewaters poses environmental threats, and a cost-effective strategy to remediate dyed water is adsorption: this process could be enhanced using nanostructured sorbents, that expose high surface areas.

Methods: In this work, chitosan aerogel adsorbents were produced by supercritical CO_2 assisted drying, working at 200 bar, 35 °C, and CO_2 mass flow rate of 0.8 kg/h. FESEM images proved that the delicate biopolymeric network was intact thanks to near-zero surface tension at the interface between CO_2 and the liquid, and large supercritical fluid diffusivity. Methyl Orange (MO) and Crystal Violet (CV) were used as model anionic and cationic dyes, respectively.

Significant findings: Changing dye initial concentration, chitosan aerogel showed different behavior at low and large driving forces, for both CV and MO. Adsorption experiments proved that MO could be not completely removed by aqueous solutions: whereas, CV removal was successful with removal efficiencies up to 89.0 ± 1.1 % from a 10 ppm solution, using 50 mg of aerogel. FT-IR analysis proved that chitosan active sites were more effectively involved with CV rather than MO. Kinetic analysis, carried out for both dyes, showed that the process follows a pseudo-second order kinetics, related to internal mass transfer resistances and diffusion phenomena.

* Corresponding author.
E-mail address: scardea@unisa.it (S. Cardea).

https://doi.org/10.1016/j.supflu.2024.106442
Received 4 July 2024; Received in revised form 27 October 2024; Accepted 27 October 2024
Available online 28 October 2024

1. Introduction

Process intensification is leading to water contamination from industrial activities [1–3]. Emerging contaminants are a specific category of compounds detected in water bodies, suspected of being toxic, thus, detrimental to environmental and human well-being [4,5]; their environmental control is not yet perfectly regulated. Such family of compounds is wide, and involves dyes, drugs, pesticides, herbicides, antibiotics, nanomaterials, chlorinated and fluorinated compounds, polymers, flame retardants, etc. [6–8]. Synthetic dyes are extensively used by industry, for their ability to fix color to different fabrics (i.e., cotton, leather, nylon, polyester, etc.) and paper. Moreover, they are resilient and resistant to chemical detergents and sunlight [9–11]. However, if not properly disposed of, they could result in severe physico-chemical alterations of water bodies, posing a threat from both an environmental and hygienic point of view [12,13]. From a chemical perspective, dyes can fall into different categories, on the basis of their specific properties: they can be non-ionic, anionic, cationic, acidic, basic, disperse, azo, diazo, etc. [14–16].

In this work, Crystal Violet (CV) and Methyl Orange (MO) were used as reference dyes. CV is cationic. On the other hand, MO is a linear anionic dye.

The abundance of such contaminants in wastewaters is pushing researchers towards the individuation of an efficient and cost-effective strategy to eliminate these synthetic dyes. Currently, several techniques have been explored in the scientific literature, such as:

- Biological treatments: they employ microorganisms (bacteria, fungi, yeasts, algae, etc.) or enzymes to biodegrade dyes using either aerobic or anaerobic processes [17].
- Chemical treatments: they are based on the utilization of reactive species to alter dyes structural stability. The most widespread chemical treatments are the Advanced Oxidation Processes (AOP), like Fenton and photo-Fenton processes or photocatalysis [18].
- Physical treatments: they are driven by mass transfer phenomena (coagulation, flocculation, membrane filtration, adsorption, etc. [19]).

Biological and chemical treatments, although appealing for their simplicity, suffer from low productivity or from slow kinetics, poor scalability, and tendency to generate reaction intermediates that are potentially more dangerous than dyes themselves. Physical treatments are the most widespread techniques to remediate water bodies, and they are massively employed from industries. Although, techniques like coagulation and sedimentation (and relative post-treatments) are not effective towards cationic and persistent water-soluble dyes, and low removal rates are obtained [20,21].

Adsorption is recommended for its scalability, simplicity, flexibility, and cost-effectiveness [22]. However, numerous parameters drive adsorption processes. For instance, chemical affinity between phases plays a pivotal role in adsorption efficiency, as well as solute stability in water: the solid phase could interact weakly with the solute (i.e., physical adsorption), or set strong chemical bonds with it (i.e., chemical adsorption) [23–25]. In addition, being adsorption a surface phenomenon, solid-fluid interfaces are involved: the higher is the adsorbent surface area, the higher it is the number of active sites offered by the solid phase (i.e., more dye could be adsorbed).

In light of these considerations, the choice of the adsorbent defines the outcome of the process: basically, the adsorbent should be compatible with the dye to remove, and it should possess high surface areas. Some adsorbents are used in the scientific literature, like metalorganic frameworks (MOFs), zeolites, etc., but they production can depend on the utilization of toxic organic solvents and time-consuming processes, defeating the purpose of intensive and sustainable production.

Chitosan (CH) – poly(β-(1−4)-*N*-acetyl-D-glucosamine) – is a natural biopolymer, obtained by the deacetylation of chitin, that is extracted by the exoskeleton of mollusks and crustaceans [26,27]. It is interesting for adsorption purposes, since it offers reactive functional groups, namely, amine and hydroxyl, employable for adsorbent-adsorbate interactions. Nevertheless, it should be noted that chitosan performance as adsorbent material strictly depends on how it is processed, thus, on its morphological architecture, structural openness, grafting active groups, filler loading, etc. For example, an effective strategy to fully exploit chitosan properties is to produce nanostructured devices: the sol-gel route, combined with supercritical CO_2 (SC-CO_2) assisted drying, is known to keep intact the chitosan delicate architecture and nanopores are wide open, thus, leading to higher surface areas, thanks to SC-CO_2 near-zero surface tension and gas-like diffusivity [28–30].

Several chitosan-based devices have been produced, and their performances have been studied towards dye removal from wastewater. As far as MO adsorption is concerned, different solutions have been tested. Zhai et al. [31] produced CH microspheres (d= 440 μm) by microfluidic technique followed by air drying: they tested different initial concentrations, ranging from 20 to 60 mg/L, using 50 mg of microspheres. Monitoring MO concentration with time, up to 300 h, they pointed out that adsorption efficiency was a function of contact time, and of adsorbent dosage. Using the Langmuir equation to extrapolate the saturation capacity (q_{max}) of chitosan beads, they obtained a value of about 207 mg/g. But, from a kinetic point of view, the authors observed that MO adsorption happened mainly on the surface; whereas, much longer times were needed for diffusion phenomena to complete. Jiang et al. [32] synthetized CH/β-cyclodextrin composites for MO removal, using maleic anhydride as a bridge between the two species. Varying solution pH, they noted that electrostatic attraction between MO and chitosan was higher in acidic conditions, when the aminic group gets protonated. Analyzing adsorption kinetics, it was highlighted that most of MO was captured in the first 50 minutes, thanks to the synergistic effect of CH and β-cyclodextrin, that hosted MO molecules. Again, a rate-limiting step was observed, and intraparticle diffusion only partially contributed to the process. The composite resulted in high saturation capacities (392 mg/g). Habiba et al. [33] produced CH/polyvinyl alcohol/zeolite electrospun fibers, aiming at clearing MO dyed water. Adsorption capacities were about 20 mg/g, and Langmuir model suggested that saturation capacity was 153 mg/g. In this case, adsorption was mainly a surface phenomenon, and intraparticle diffusion did not affect the outcome: as a proof of this observation, it was noted that equilibrium was reached in few-minutes. Overall, MO dye can be adsorbed by CH-based materials, but kinetics is influenced by morphology, architecture, and textural properties. Indeed, MO is a linear molecule that could find some obstruction in the tortuosity of nanostructures.

Also CV removal by CH-based systems has been explored. Vithalkar et al. [34] produced CH/bentonite spheres by pH-induced gelation and air drying. CV was almost completely removed from the starting solution using 50 mg of composite, in less than an hour. Massoudinejad and coworkers [35] evaluated the efficiency of chitosan adsorbents loaded with a Fe_3O_4 nanopowder. In this case, the optimal combination of adsorption parameters were: initial concentration 77 mg/L, contact time 140 min, and adsorbent dosage 1 g/L, processing 100 mL solutions. Such conditions led to a CV removal of 71.5 %. Under the assumption that monolayer adsorption took place, the saturation capacity was evaluated to be about 333 mg/g. The same authors suggested that CV could be adsorbed onto CH surface thanks to -OH and -NH_2 functional groups, which bonded with the cationic part of CV. Other porous devices were proposed for CV removal, like chitosan/graphene oxide/polyurethane foams [36]. CV initial concentrations ranged from 100 to 300 mg/L, when adsorbent dose was set at 50 mg/mL to treat 10 mL solutions. Almost all CV was removed from the starting solution; but, it is noteworthy that saturation capacity was estimated to be around 64.9 mg/g. It is possible that the produced composite did not show high chemical affinity with the dye, or that foams, being structurally closed, did not offer an open network for the solute to move through.

The scientific literature does not report any attempt to use nanostructured chitosan aerogels for MO or CV removal. Consequently, the scope of the present work was to assess, for the first time, the comparison between MO and CV removal using chitosan aerogels produced via SC-CO_2 assisted drying. Moreover, the aim was also to explore the features of nanostructured sorbents for wastewater treatment. Different chitosan concentrations and molecular weight were considered to find the best candidate for adsorption purposes; then, once the optimal combination was chosen, the effect of initial concentration on dye uptake was studied, and the related thermodynamical and kinetic analyses are presented.

2. Materials and methods

2.1. Materials

Chitosan, both medium and low molecular weight (MMW and LMW, deacetylation degree ≥75 %, viscosity 200–800 and 20–300 cps, respectively) were purchased from Sigma Aldrich (St. Louis, MO). Also glacial acetic acid (purity ≥99 %) and sodium hydroxide (NaOH, reagent grade, purity ≥97.0 %, pellets, anhydrous) were obtained from Sigma Aldrich. Distilled water was produced using a lab-scale distillation column.

CO_2 (99.9 % pure) was supplied by Morlando Group Srl (Napoli, Italy). Methyl orange (dye content 85 %) and crystal violet (≥90.0 % anhydrous basis) were bought from Sigma Aldrich (St. Louis, MO). Chemical formula and structure of the dyes used in this work are reported in Table 1.

2.2. Chitosan hydro- and solvo-gels preparation

MMW and LMW chitosan hydrogels were produced using three CH concentrations: 1, 3 and 5 % w/w. Chitosan powder was solubilized in acidic water (3 % v/v acetic acid) and stirred at 200 rpm for half an hour until complete solubilization. Once the polymeric solution was obtained, sol-gel transition was induced by solution basification: NaOH 1 M aqueous solution was added dropwise until pH increased up to 12–13. pH was monitored using a pH-meter (Hanna Instrument, mod. HI 2210). Chitosan hydrogels were rinsed using distilled water to remove residual salts. Since SC-CO_2 and water are immiscible, water had to be swapped with ethanol: 10, 30, 50, 70, and 90 % v/v ethanol/water solutions were prepared and put in contact with the hydrogel for 1 hour each. In the end, the contact with pure ethanol was prolonged overnight, to ensure complete water substitution: the solvogel was obtained.

2.3. Aerogel production using supercritical drying

Supercritical drying was performed in a lab-scale apparatus: the 200 mL steel high-pressure vessel where solvogels were located was set at 200 bar and 35 °C for every experiment. CO_2 mass flow rate was set at 0.8 kg/h. Such operating conditions were chosen based on previous drying experiments carried out on chitosan structures [28,30]. A refrigerating bath (Julabo, mod. ED-F35) was used to bring CO_2 to the liquid state before entering the high-pressure pump (Gilson, mod. 146562), that was used to reach the desired pressure. CO_2 was pre-heated and sent to the drying vessel, whose temperature was controlled using heating bands regulated by a PID controller (Watlow, mod. 93). The mixture CO_2-ethanol was separated in a vessel down the line, operating at atmospheric conditions: ethanol was collected at the bottom of the vessel, while CO_2 was released. Pressure was regulated manually using a micro-metering valve (Milli-Mite 1300 Series HOKE), and CO_2 flow rate was monitored by a calibrated rotameter. Pressure and temperature were continuously monitored along the line, using test gauges and thermocouples, respectively. Each drying lasted about 6 hours, and once it was over, the system was slowly brought to atmospheric conditions. Then, the aerogels were collected. Each experiment was replicated at least three times.

2.4. Point of zero charge (PZC) measurement

The point of zero charge is the point at which the solid bears no charge on its surface. It was measured using the procedure suggested by Kumar and Jiang [37] with slight modifications: a 0.01 M NaCl solution has been prepared, and 0.1 M HCl and NaOH solutions were used to adjust initial pH. 20 mg of aerogel were located in 40 mL of solution stirred at 300 rpm, and an equilibration time of 24 h was waited before pH measurement. Final pH was measured on the filtrate, and pH variation calculated as pH_i-pH_f. The plot of pH_i-pH_f vs. pH_i was obtained, and PZC calculated as the pH_i value at which pH_i-pH_f was equal to zero.

2.5. Characterizations

Morphological analyses were carried out by field emission scanning electronic microscopy (FESEM, Carl Zeiss Supra 35). Aerogel sections

Table 1
MO and CV chemical formula and structure.

Dye	Chemical formula	Structure
Methyl Orange	$C_{14}H_{14}N_3NaO_3S$	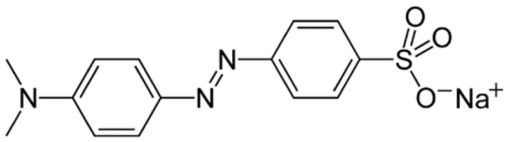
Crystal Violet	$C_{25}N_3H_{30}Cl$	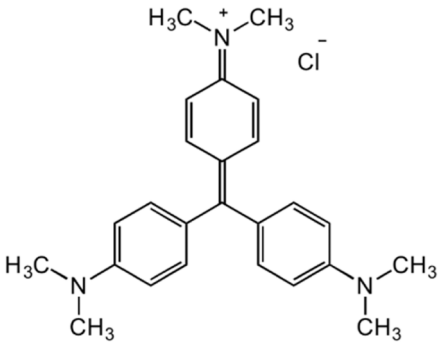

were obtained by cryofracturing the sample in liquid nitrogen, to avoid structure deformation. At least three sections were investigated from each analyzed aerogel, to check morphological homogeneity. Samples were coated with gold, using an Agar Auto Sputter Coater (mod. 108 A, Stansted, UK). Fourier Transform-Infrared Spectroscopy (FT-IR, IRTracer-100, Shimadzu) was carried out once a solid mixture of sample and KBr (1:100 w/w) was finely grinded and shaped as a thin semi-transparent disk, using a hydraulic press. Scans resolution was 32 cm^{-1}. Brunauer-Emmett-Teller (BET) Specific Surface Area (SSA) and Barrett-Joyner-Halenda (BJH) measurements were carried out using 77 K nitrogen adsorption on 200 mg samples, by the instrument Nova 1200e Surface Area (Quantachrome Instruments, Boynton Beach, FL, USA). The applied method was the one proposed by Tabernero and co-workers [30]. Pore size distribution was evaluated using ImageJ as analysis software.

2.6. Adsorption experiments

Adsorption experiments were performed batch-wise, using 50 mg of chitosan aerogel in a 50 mL dye solution of different initial concentration. The investigation of the effect of the driving force on adsorption was divided in two steps: firstly, low initial concentrations, like 1, 5, and 10 ppm were tested; then, a high-concentration range was analyzed, using dye solutions of 25, 50, and 100 ppm. Larger dyes initial concentrations were not tested due to MO and CV solubilization issues. Dynamic Light Scattering (DLS, mod. Zetasizer Nano S, Worcestershire, United Kingdom) analysis was performed to check dye clustering in solution.

Aerogels were loaded into a teabag to avoid material dispersion and inefficient contact between the solution and the adsorbent. The system was stirred at 200 rpm to guarantee composition homogeneity. MO or CV concentration was monitored using a UV-Vis spectrophotometer (Model Cary 60, Varian, Palo Alto, CA, USA). Prior to batch experiments, calibration curves were obtained reading the absorbance of test solutions at a wavelength of 460 nm for MO and at 590 nm for CV. The calibration curves used in this work were Eq. (1) and Eq. (2), respectively, for MO and CV, where A is the absorbance and C the concentration.

$$A=0.75\cdot C \tag{1}$$

$$A=0.18\cdot C \tag{2}$$

The results were collected using the following nomenclature: "C_{eq}" is referred to as the dye (MO or CV) plateau value the solution reached after equilibrium; "C0" is the initial concentration; "q" is the amount of dye the adsorbent took up after the experiment, calculated as reported in Eq. (3):

$$q = \frac{C_0 - C_{eq}}{m_{chitosan}} \bullet V_{solution} \left(mg \Big/ g\right) \tag{3}$$

Consequently, q_{eq} is the mass of dye taken up per unit of adsorbent, after equilibrium was reached. Removal efficiency was named "η", and it was calculated as indicated in Eq. (4).

$$\eta = \frac{C_0 - C_{eq}}{C_0} \bullet 100 \tag{4}$$

All experiments were carried out at room conditions and spontaneous pH (i.e., about 7), and performed in triplicate.

2.7. Isotherm and kinetic analysis

In this work, attempts to describe thermodynamical behavior and kinetics analysis have been carried out. As far as isotherms are concerned, the most frequent models used to fit adsorption equilibrium points are Langmuir and Freundlich isotherms [38]. Langmuir isotherm can be expressed in the linearized form (Eq. (5)).

$$\frac{C_{eq}}{q_{eq}} = \frac{1}{q_{max} \bullet K} + \frac{C_{eq}}{q_{max}} \tag{5}$$

On the other hand, Freundlich isotherm follows Eq. (6):

$$q_{eq} = k_f \bullet C_{eq}^{\frac{1}{n}} \tag{6}$$

Freundlich isotherm was linearized in a semi-logarithmic scale. A linear regression analysis was carried out as the result of an in-built statistic calculus on the software Origin 2018.

The same logic applies to kinetics analysis and, although several kinetic models are proposed in the scientific literature, the most frequent ones are the pseudo-first order, also known as Lagergren kinetics, and the pseudo-second order kinetics (Blanchard model) [38,39]. Lagergren model was used in its linearized form in a semilogarithmic scale (Eq. (7)).

$$\ln\left[q_{eq} - q(t)\right] = -k_1 t + \ln q_{eq} \tag{7}$$

On the other hand, the pseudo-second order kinetics was used in the following form, indicated in Eq. (8):

$$\frac{t}{q(t)} = \left(\frac{1}{q_{eq}}\right) t + \frac{1}{k_2 {q_{eq}}^2} \tag{8}$$

Linear regression was carried out the same way of the isotherm analysis.

3. Results and discussion

3.1. Chitosan aerogels

Prior to adsorption experiments, different combinations of chitosan concentrations and molecular weights were tested, to produce a CH aerogel that meets the need for structural openness (to guarantee solute diffusion and adsorption) and mechanical stability. Namely, 1, 3 and 5 % w/w aerogels were produced, using both LMW and MMW chitosan. All dried gels did not undergo significant shrinkage after supercritical drying. Overall, hydrogels, solvogels, and aerogels showed approximately the same volume.

However, 1 % w/w LMW chitosan aerogels could not be produced: the gelation phase failed. This result could be related to the fact that chitosan could not rearrange in a stable configuration, due to chains length. Fewer entanglements and less intense interactions were formed in the polymeric solution: consequently, a strong gel and an interconnected network could not be formed.

In Fig. 1, it is reported a collection of the most representative FESEM images of LMW chitosan aerogel section, on both the microscale and nanoscale.

FESEM images reported in Fig. 1 show that at all concentration tested, the landscape of aerogels cross-section at a microscopic level was fiber-like, open and interconnected.

5 % w/w LMW CH aerogels were morphologically more compact and closed than 3 % w/w ones, although regular on every scale. It is noteworthy that during gelation, 5 % w/w CH solutions were extremely viscous, and NaOH could not diffuse uniformly in the inner core of the solution itself: longer times were needed to ensure sample gelation. Structural closure on the microscale means larger mass transfer resistances towards water diffusion, while on the nanoscale could result in active sites unavailability for adsorption. It must be highlighted that supercritical drying allowed to keep intact chitosan network in each case, even though structural stability was compromised by chains length.

Fig. 2 shows some FESEM images of MMW CH aerogels cross sections. Differently from LMW CH gels, in this case 1 % w/w MMW CH was successfully produced: this result represents a further indication of the connection between chains length and gelation properties of the system.

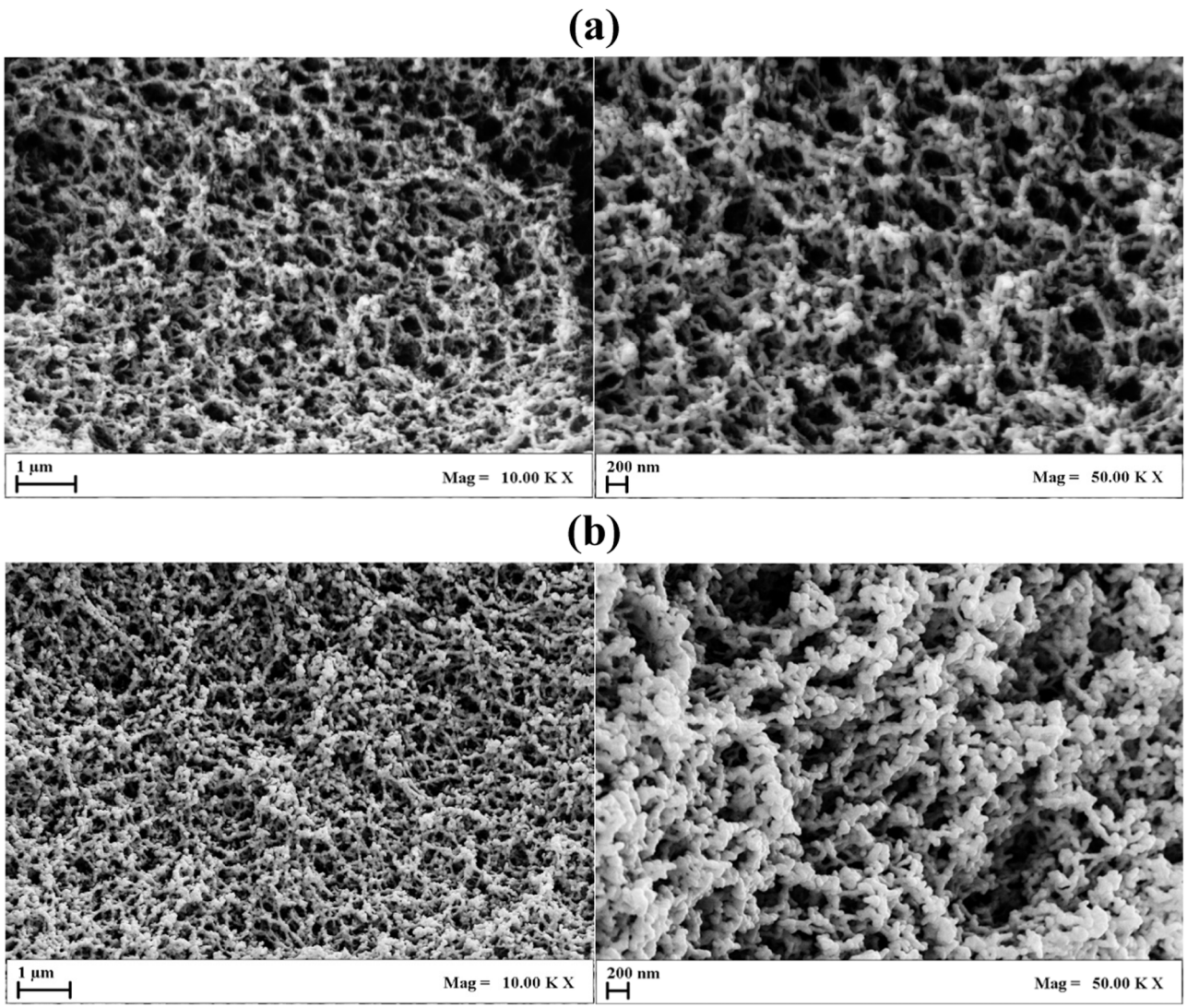

Fig. 1. FESEM images of LMW chitosan aerogel cross section: (a) 3 % w/w; (b) 5 % w/w.

Looking at Fig. 2, the same considerations performed for LMW aerogels can be applied to MMW ones. Also in this case, nanostructure was not disturbed during solvent extraction, thanks to SC-CO_2 gas-like properties. Increasing polymer concentration, aerogels cross section became more clustered. This trend is amplified for 5 % w/w MMW CH aerogels, where polymer aggregation phenomena are more evident. Wider voids were formed, but there are regions in which chitosan concentration is higher and the corresponding configuration is more compact, compromising active sites availability for adsorption. Therefore, polymer clustering can show a negative effect on process thermodynamics, meaning that the maximum adsorption capacity could be lowered due to active sites unavailability. On the other hand, also kinetics can be affected by polymer aggregation: wider pores are present in high-concentration systems, that can lead to faster solution diffusion rates and shorter process times – but, it is also associated with smaller dye uptakes. Also, for 5 % w/w MMW CH gels, viscosity was extremely high, and compromised system processability and fast and complete gelation. In contrast, 1 % w/w MMW CH aerogels were easy to handle, and from a morphological perspective, they were extremely open and regular also on the microscale. However, these samples should be discarded for adsorption experiments due to the lack of mechanical resistance. Low concentration aerogels were extremely fragile, and they flaked when handled. Other indication of the differences between MMW CH aerogels is related to fibrils' thickness at all magnitudes. It can be seen that polymer concentration does not affect only samples openness and regularity, but also fibrils are progressively thinner decreasing CH concentration. However, for adsorption experiments, it should be found a compromise between aerogel bulk stability and morphological openness. Moreover, SSA measurements were carried out. The results are synthetized in Table 2.

As reported in Table 2, the sample that offers the largest SSA is 3 % w/w MMW aerogel. Therefore, it is the aerogel richer in active sites available for adsorption. Being the most promising candidate for this purpose, 3 % w/w MMW chitosan aerogels were further characterized, and their BJH pore size evaluated: the value was estimated to be 12 ± 1 nm.

Looking at the combinations of CH molecular weights and concentrations analyzed, the following considerations were carried out:

- Fixing CH concentration, fibrils are thicker and pores more closed when molecular weight is increased. Chains arrangement affects not only morphological configuration, system interconnection and voids width, but also mechanical resistance. Low molecular weight samples were broken more easily when handled, with respect to high molecular weight samples at the same concentration.
- Hydrogels processability and overall structural compactness allows to discard high-concentration systems, for both LMW and MMW samples: polymer clustering could compromise active sites

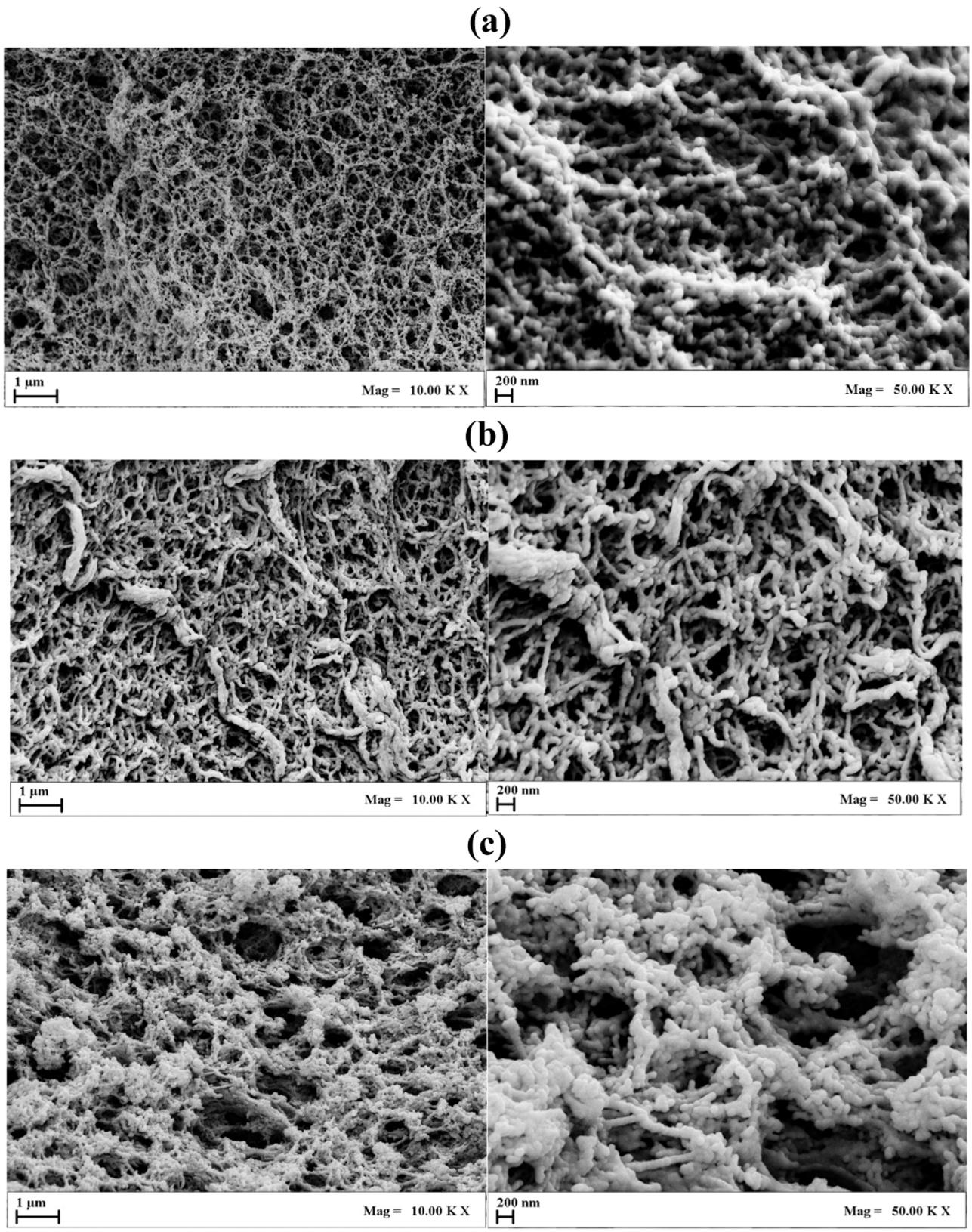

Fig. 2. FESEM images of MMW CH aerogel: (a) 1 % w/w; (b) 3 % w/w; (c) 5 % w/w.

availability, causing an obstacle for solute interactions with the functional groups of chitosan. 5 % w/w gels were not further considered in the present work.

- When low CH concentrations (1 % w/w) were processed, sample either could not undergo gelation, namely, for LMW solutions, or, after SC-CO_2 drying did not form a stable structure (MMW samples).

Table 2
Chitosan aerogels SSA.

	SSA, m^2/g	
Chitosan concentration	**LMW chitosan aerogels**	**MMW chitosan aerogels**
1 % w/w	N.A.	57.9 ± 6.1
3 % w/w	84.0 ± 3.0	118.2 ± 10.2
5 % w/w	103.0 ± 7.0	74.7 ± 5.3

- 3 % w/w CH aerogels (both LMW and MMW) were the most promising candidates for adsorption. They both showed hierarchical regularity and a highly interconnected architecture, crucial for homogeneous solute diffusion in the network. However, in this first-basis analysis, the choice fell on MMW aerogels, due to their more stable bulk configuration, although compact: see comparison between Figs. 1a and 2b). Indeed, 3 % w/w LMW aerogels could be compounded with stabilizing fillers, thus, improving mechanical toughness, but it was not the focus of the present study.

Overall, 3 % w/w MMW CH aerogels were selected since they filled the gap between mechanical resistance and morphological regularity and network interconnection, and showed the largest SSA. To further characterize this aerogel sample, Image analysis was carried out to determine pore size distribution: pores of the prepared 3 % w/w MMW chitosan aerogel result to have a mean diameter of about 270 ± 48 nm.

3.2. Point of zero charge

The PZC was measured accordingly to the procedure described in *Materials and Methods* section. Fig. 3 reports the plot pH_i-pH_f vs. pH_i.

The PZC parameter is essential for understanding adsorption phenomena. Namely, it is the point above which the solid surface is negatively charged; whereas, below the PZC value, it bears an excess of positive charge. Looking at Fig. 3, it can be seen that PZC for the produced chitosan aerogels is about 7, coherently with literature data [37, 40,41]. At pH>7, chitosan surface strongly interacts with cationic dyes such as CV, which are positively charged. On the other hand, at pH<7, chitosan surface interacts more effectively with anionic dyes. Consequently, chitosan aerogels can adsorb cationic and anionic dyes on the basis of solution pH.

3.3. Methyl Orange adsorption

3.3.1. MO adsorption experiments

MO adsorption experiments were carried out considering two ranges of initial concentration, namely: low initial concentration (1, 5, and 10 ppm), and high initial concentration (25, 50, and 100 ppm). In both cases, performing DLS analysis on the prepared solutions, there was no evidence of MO clustering. The reason behind this approach, is related to the effect of the driving force on dye uptake: even though nanostructures offer higher surface areas and more abundant active sites for adsorption, tortuosity could represent a consistent obstacle for dye removal. Potentially, such mechanism is valid also if MO steric hindrance does not allow effective diffusion in the nanostructure. This effect could be enhanced for low driving forces, since the solute is adsorbed first on the solid surface, and later on in the inner structure. The results of the MO adsorption experiments are graphically reported in Fig. 4.

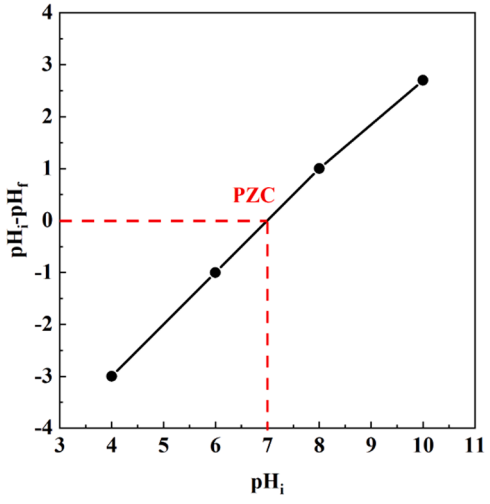

Fig. 3. Chitosan aerogel PZC.

Looking at the experimental points collected at low concentrations (Fig. 4a), it can be pointed out that the plateau value was reached in about 1–2 hours; whereas, higher concentrations (Fig. 4b) needed longer times to balance the driving force between the liquid bulk and chitosan surface. MO uptake was unsatisfying for low concentrations: the potentiality of the nanostructure was not fully employed. Experiments at larger C_0 were crucial to understand whether CH aerogel and MO were non-compatible from a chemical perspective, or the kinetic effect was dominant for nanostructured devices. Indeed, also the adsorption experiments carried out at 25, 50 and 100 ppm showed some improvements, but MO was not satisfyingly removed from the dyed solution.

Table 3 reports a brief summary of the results on these experiments, collected once plateau values were reached.

From the data reported in Table 3, it can be observed that q increased by increasing MO initial concentration: the effect of the driving force on the adsorption capacity followed the expected trend. However, it is worth to focus the attention on η: at first, for low concentrations, removal efficiency decreases, as if the aerogel reached its saturation capacity. However, increasing the driving force using higher C_0, removal efficiency increases up to about 29.2 ± 1.3 %, although there were not significant changes when moving from 25 to 100 ppm. If η decreased, it could have been the effect of reaching the adsorbent saturation capacity: however, being overall constant, it could mean that MO did not diffuse efficiently in CH nanostructure, although active sites were available for adsorption.

This first set of adsorption experiments led to the conclusion that the partial inefficiency of the process, using 50 mg of aerogel, could be related to the difficulty for the MO dye to diffuse inside the aerogel, and not to the unavailability of active sites. Indeed, from a chemical perspective, it was proved by previous studies, that chitosan works as an efficient adsorbent towards methyl orange. It was also pointed out that MO adsorption takes place mainly on the external surface: diffusion inside the adsorbent structure can be eased using, for instance, β-cyclodextrins [32], which could provide a preferential route for the dye to follow.

3.3.2. MO adsorption isotherm

To further understand the mechanisms behind MO adsorption on CH nanostructures, equilibrium points were collected (Fig. 5), to obtain the adsorption isotherm.

Fig. 5 graphically reports data in Table 3: the system behaves differently at low and high concentrations. Employing this kind of nanostructured adsorbent, the system reached a point at which, for low concentrations, MO could not diffuse further in the chitosan network; however, larger initial concentrations pushed more efficiently the dye in the adsorbent, improving the adsorption capacity. Moreover, the equilibrium values did not seem to approach the plateau value. In the range of concentrations tested, the system did not reach the maximum saturation efficiency, meaning that the nanostructure could still host MO molecules. However, as mentioned in the *Materials and Methods* section, it was not possible to test larger MO initial concentration due to its low solubility at concentration higher than 100 ppm. Therefore, plateau equilibrium values could not be obtained. Table 4 reports the results of

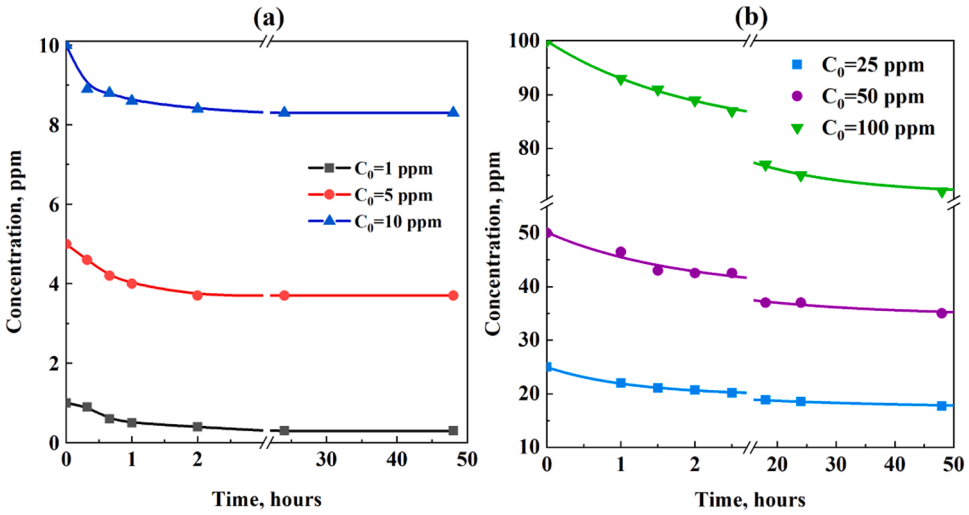

Fig. 4. MO adsorption at: (a) C_0=1, 5 and 10 ppm; (b) 25, 50 and 100 ppm.

Table 3
Results of MO adsorption experiments.

C_0, ppm	C_{eq}, ppm	q_{eq}, mg/g_{ads}	η
1.0 ± 0.1	0.3 ± 0.1	0.7 ± 0.2	70.0 ± 13.0 %
5.0 ± 0.1	3.7 ± 0.1	1.3 ± 0.2	26.0 ± 3.4 %
10.0 ± 0.1	8.3 ± 0.1	1.7 ± 0.2	17.0 ± 1.8 %
25.0 ± 0.2	17.7 ± 0.2	7.3 ± 0.4	29.2 ± 1.3 %
50.0 ± 0.2	35.5 ± 0.3	14.5 ± 0.5	29.0 ± 0.8 %
100.0 ± 0.3	72.0 ± 0.3	28 ± 0.7	28.0 ± 0.5 %

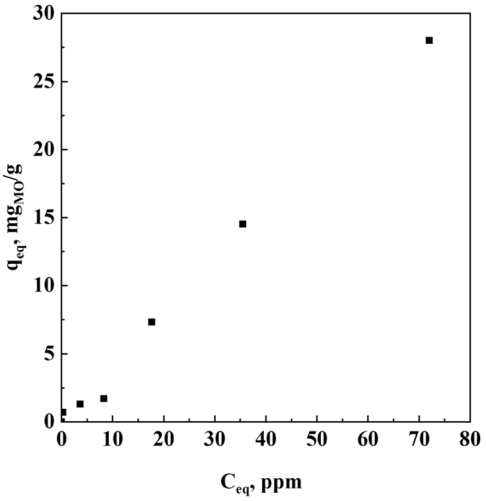

Fig. 5. MO adsorption equilibrium points.

Table 4
Langmuir and Freundlich parameters for MO adsorption.

	Langmuir			Freundlich		
	K, L/mg	**q_{max}, mg/g**	**R^2**	**k_f, (mg/g)(L/g)$^{1/n}$**	**n**	**R^2**
Low concentration	3.92	1.81	0.98	0.95	3.81	0.99
High concentration	0.001	356.8	0.97	1.02	1.08	0.99

the attempts to fit the equilibrium points using Langmuir and Freundlich isotherms. Since the system behaved differently at low and high concentrations, it was chosen to separate the analysis in the respective ranges of C_0. To obtain the correlation coefficients of the mentioned models, the mean values of C_{eq} and q_{eq} have been considered.

The values of R^2 reported in Table 4 show that this system is more correctly described by the Freundlich isotherm, in all ranges of concentration tested. However, it is worth to mention that even though Langmuir isotherm does not show the highest R^2, for high concentrations it extrapolates a saturation capacity of 356.8 mg/g. For both models, it can be highlighted the gap between the parameters of low and high driving forces scenarios, proving that the system behaves differently in such cases. For instance, focusing the attention on the Freundlich isotherm, that is the best-fitting model in this case – see the linearized equation in *Materials and Methods* section – it can be pointed out that the higher is k_f, the larger is the amount of dye adsorbed per mass unit of adsorbent: indeed, k_f is higher for high concentrations than it is for low ones. On the other hand, the effect of "n" could be different depending on the values of C_{eq}: if C_{eq} falls between 0 and 1, the decrease of n, thus an increase of 1/n, determines a drastic reduction of q_{eq}, meaning that adsorption was overall compromised. On the other hand, for larger C_{eq}, the higher n is, the lower is its inverse and the lower is the amount of MO adsorbed at equilibrium conditions.

Although the results obtained in this work for MO adsorption seem to be improvable, they can be compared with others mentioned in the *Introduction*. Indeed, maximum monolayer capacity for chitosan aerogels (356.8 mg/g) is much higher than the one calculated for chitosan microspheres [31] (i.e., 207 mg/g). Although adsorption efficiency is larger for the latter case (MO was almost completely removed from the starting solution), it is worth noting that the plateau value was achieved in 300 hours rather than the 1–2 hours needed in the present work. It can be also pointed out that other systems result in faster adsorption rates and larger monolayer capacities [32], their fabrication employs toxic crosslinkers and organic solvents, that weigh negatively on the whole process sustainability: different aspects must be taken into account when it comes to the choice of the most eligible adsorbent for dye removal. Also, the adsorbents produced by Habiba et al. [33] have lower adsorption capacities, but the process takes place in a few minutes timespan. Indeed, by comparing the outcomes of this work with others reported in the literature, it can be stated that, although improvable, the formers are also promising with respect to other chitosan-based composites.

3.4. CV adsorption

3.4.1. CV adsorption experiments

Coherently with MO results, also CV adsorption experiments were carried out separating low-concentration (1, 5 and 10 ppm) steps and high-concentration (25, 50, 100 ppm) ones. Also in this case, DLS analysis was performed on the prepared solution, and no particle size distribution was recorded, meaning that CV did not cluster in the range of concentrations tested. Fig. 6 reports the results obtained for these experiments.

Notably, the system is much more efficient for CV than for MO. Moreover, experimental points reached their plateau value in a maximum of three hours for both concentration ranges, apart from 5 and 1 ppm (Fig. 6a), which reached the plateau, respectively, in 1 and half hours. 1 ppm solution was completely cleared after adsorption; whereas, the other samples were not completely decolored, but a significant reduction was detected. Equilibrium points were collected for these adsorption experiments and reported in Table 5.

The values of q_{eq} were overall linear with the initial concentration: there is a direct dependency between the driving force and the amount of CV adsorbed during the process. Also, removal efficiencies were high for all the experiments, and it should be remarked that such results were accomplished using only 50 mg of chitosan aerogels: the process was fast and effective, especially when compared with MO adsorption. The mechanism that could stand behind these results is that CV is much more compatible with chitosan than MO, from both a chemical and a steric point of view. However, from a chemical point of view, PZC proved that chitosan aerogels can interact with CV and MO at their spontaneous pH. CV solution pH is basic; whereas, MO is acidic. For this reason, the inefficiency of MO removal can be attributed to its linear structure, that may be an obstacle to dye diffusion in the chitosan internal nanostructure. On the other hand, CV is not a linear dye, and this difference in steric disposition affects adsorption process. Indeed, the adsorbent nanostructures were better employed for CV adsorption rather than MO.

3.4.2. CV adsorption isotherm

Also for CV adsorption, an attempt to extrapolate isotherm curves was carried out. Both Langmuir and Freundlich models were tested for the two separate concentration ranges. The q_{eq} vs. C_{eq} points are reported in Fig. 7, taking into account the data collected in Table 4. Similarly to MO, also CV adsorption could not be assessed at concentrations larger than 100 ppm due to scarce solubilization.

Once again, the q_{eq} vs. C_{eq} points seem to behave differently in the low and high concentration range: at first, adsorption happened efficiently. Indeed, CV adsorption on CH aerogels did not suffer from kinetic limitations or steric hindrance, and the adsorbent was employed correctly, even at small driving forces. However, the trend reversed for high concentrations, from 25 to 100 ppm, as if the adsorbent begun to saturate for larger driving forces. Furthermore, the system did not approach to the equilibrium value in the range of concentrations tested.

As far as the isotherm fitting was concerned, the linearization of q_{eq} vs. C_{eq} points was not possible through the Langmuir model for the high concentration data. The isotherm parameters did not have physical meaning: namely, negative slope was obtained. Consequently, the value of q_{max} was negative, and it was not acceptable from a phenomenological perspective. Table 6 collects the most relevant results of the fittings.

Looking at the different parameters of the two models, it can be

Table 5
Results of CV adsorption experiments.

C_0, ppm	C_{eq}, ppm	q_{eq}, mg/g_{ads}	η
1 ± 0.1	0.0 ± 0.0	1.0 ± 0.1	100.0 ± 0.0 %
5 ± 0.1	0.7 ± 0.1	4.3 ± 0.2	86.0 ± 2.2 %
10 ± 0.1	1.1 ± 0.1	8.9 ± 0.2	89.0 ± 1.1 %
25 ± 0.2	6.5 ± 0.1	18.5 ± 0.4	74.0 ± 0.6 %
50 ± 0.2	11 ± 0.2	39.0 ± 0.5	78.0 ± 0.5 %
100 ± 0.3	22 ± 0.3	78.0 ± 0.9	78.0 ± 0.4 %

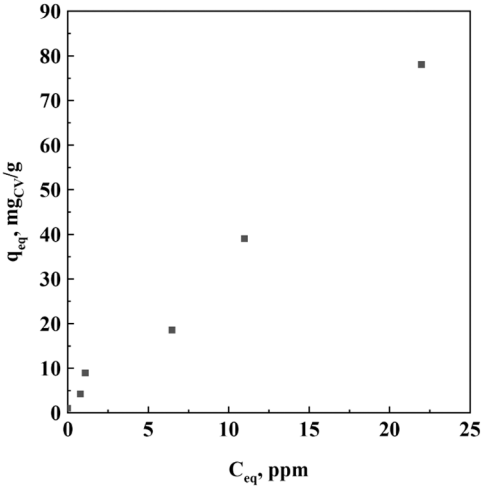

Fig. 7. CV adsorption equilibrium points.

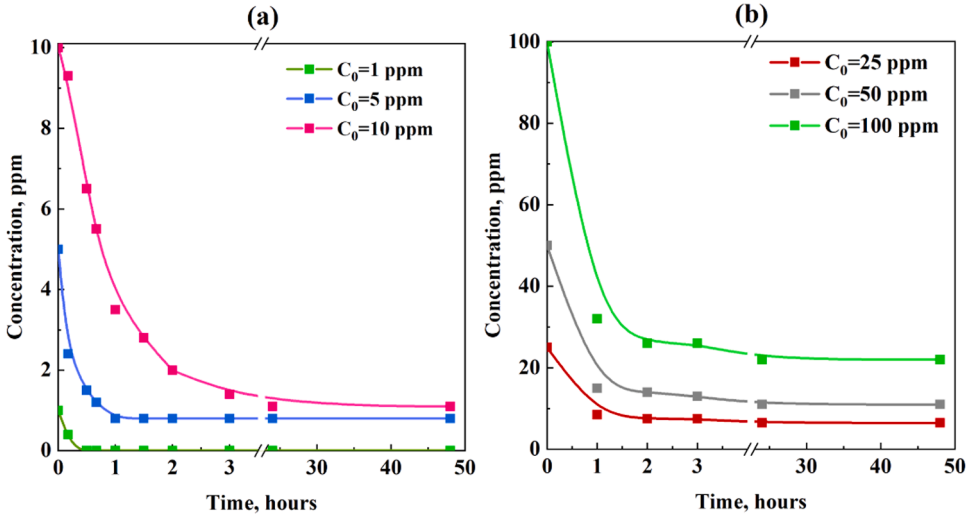

Fig. 6. CV adsorption at: (a) C_0=1, 5 and 10 ppm; (b) 25, 50 and 100 ppm.

Table 6
Langmuir and Freundlich parameters for CV adsorption.

	Langmuir			Freundlich		
	K, L/mg	q_{max}, mg/g	R^2	k_f, (mg/g)$(L/g)^{1/n}$	n	R^2
Low concentration	0.03	8.14	0.703	0.26	1.28	0.999
High concentration	N.A.	N.A.	N.A.	0.53	1.18	0.99

pointed out that Langmuir model was not a good fit for the system CV-chitosan: for this reason, it was not possible to extrapolate saturation capacity at high concentration, even though at low concentrations it provided a value of q_{max} consistent with the experimental data. On the other hand, Freundlich was much more accurate (R^2= 0.99). Indeed, it could be the sign of an energetically heterogenous adsorption, possibly coherent with the fact that the adsorbent hosted differently dye molecules: adsorption on the outer surface was facilitated by lower mass transfer resistances; whereas, solute capture on the inner nanostructure was hindered by biopolymer tortuosity. The results related to CV removal using nanostructured chitosan aerogels are promising when compared to some representative literature data. It is important to mention that maximum adsorption capacity can't be used as a quantitative reference result for comparison purposes, due to Langmuir poor fit to this system at high concentrations. However, being this value large for MO capture (i.e., 356.8 mg/g), it can be expected to be much larger for CV due to the overall better results. Indeed, the monolayer capacity of the systems reported in the state of the art (see *Introduction*) are generally low: among these works, the maximum value reported is 333 mg/g [35] - obtained using magnetic chitosan nanocomposites. The results obtained in this latter work are comparable to the ones reported in the present paper: but, confronting the Freundlich isotherm parameters for both systems, the value of 1/n is greater in this work (i.e., 0.85) than in the case of the magnetic composites (i.e., 0.74). This means that, although the aerogel produced in this work are not compounded with nanofillers, adsorption can be more favorable thanks to the 3D-nanostructured network.

3.5. FT-IR analysis

FT-IR analysis is useful to check the hypothesis formulated after the adsorption experiments: the study of the characteristic bands of the observed species led to understand whether all the active sites of the adsorption were employed. FT-IR spectra of the chitosan aerogel, of the dyes, and of the aerogel post-adsorption experiments, are reported in Fig. 8. Enlargements are also provided in Fig. 9.

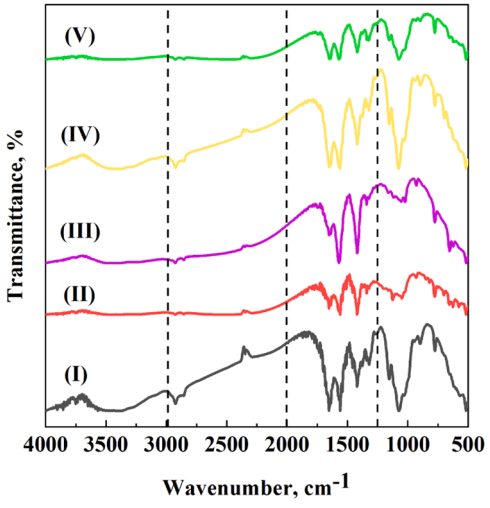

Fig. 8. FT-IR spectra of: (I) CH aerogel; (II) MO; (III) CV; (IV) CH post MO adsorption; (V) CH post CV adsorption.

First of all, the spectrum of the chitosan aerogel was used as reference, since there were not significant changes in the characteristic bands of the chitosan powder and chitosan aerogel. Previous works proved that supercritical drying does not modify the material chemistry [29]. As far as chitosan (Fig. 8a) is concerned, the broad band around 3400 cm^{-1} can be associated with -OH and -NH_2 stretching vibrations; the one present at around 2800 cm^{-1}, was, instead, related to C-H stretching, typical of polysaccharides. The bands at 1650 and 1640 cm^{-1} were related to carbonylic residues of the deacetylation process and aminic group; whereas, the one at 1376 cm^{-1} was associated with methyl groups. At last, the bands behind these regions were associated with C-O-C and C-O vibrations [28].

On the other hand, MO and CV spectra (Fig. 8b and Fig. 8c) did not show any sign of residual humidity, by looking at the left side of the graphs; but, they responded to the analysis with characteristic sharp bands in the region 2000–1250 cm^{-1}, typical of C-N vibrations (1296 cm^{-1}) of the azo dyes, and C═C stretching vibrations of aromatic nuclei (1588 cm^{-1}). Even though these two dyes shared some chemical bonds, they differed for some of them. For instance, MO possesses double-bonded nitrogen atoms (-N═N-), whose band can be found at 1607 cm^{-1}; moreover, also S═O stretching vibrations were detectable at 624 cm^{-1}, although in the fingerprint region [42,43].

Once the most relevant bands of the dyes and of the adsorbents were highlighted, it was possible to characterize the post-adsorption samples: chitosan aerogels underwent partial modification from a chemical perspective. Indeed, looking at Fig. 8d and Fig. 8e, it is possible to subdivide the spectra in different regions: moving from the right to the left of the spectra, there were not significant changes in the chitosan chemistry. Indeed, the fingerprint region was virtually identical, as well as the region between 2000 and 1250 cm^{-1}. Small changes were detected in the third region (3000–2000 cm^{-1}): after both MO and CV adsorption, C═O groups signals were a bit weaker, meaning that they were partially involved in the adsorption process. Nevertheless, the most significant variation in the chitosan spectrum was the one related to the broad band of -OH and -NH_2 groups (the last region on the left). It is noteworthy that, after MO adsorption, chitosan aerogel only partially weakened this band. Biopolymer active sites were not effectively involved in bonding with the dye; otherwise, the spectrum would have flattened. The aminic group of chitosan, notably the most reactive one, could bond more efficiently with MO if it was charged positively (i.e., if chitosan was protonated). On the other hand, if protonated, chitosan could solubilize in aqueous solution and break down. In this work, chitosan was not used in its protonated form, and MO did not bond effectively with chitosan itself, justifying the low removal efficiencies detected in the adsorption experiments. In contrast, looking at the same region in the post CV adsorption chitosan spectrum (Fig. 8e), the -OH and -NH_2 band was virtually flat: available active sites were employed for adsorption, in accordance with the experimental data obtained in the first part of the work.

3.6. Kinetics analysis

A short kinetic analysis was carried out, to have a comparative understanding of the mechanisms laying behind the adsorption of MO and CV. As a reference, the dataset obtained for 10 ppm adsorption experiments were considered for this analysis, taking into account the mean values obtained during the experiments. It should be noted that the pseudo-second order model could be easily linearized, and the value of the equilibrium capacity q_{eq} is, in both cases, coherent with the value experimentally obtained. On the other hand, the determination of q_{eq} for the Lagergren model is bound to a trial-and-error procedure, by setting q_{eq}, thus calculating the fitting parameters until the error between q_{eq} hypothesized and the one calculated fell below 10 %. The results of the

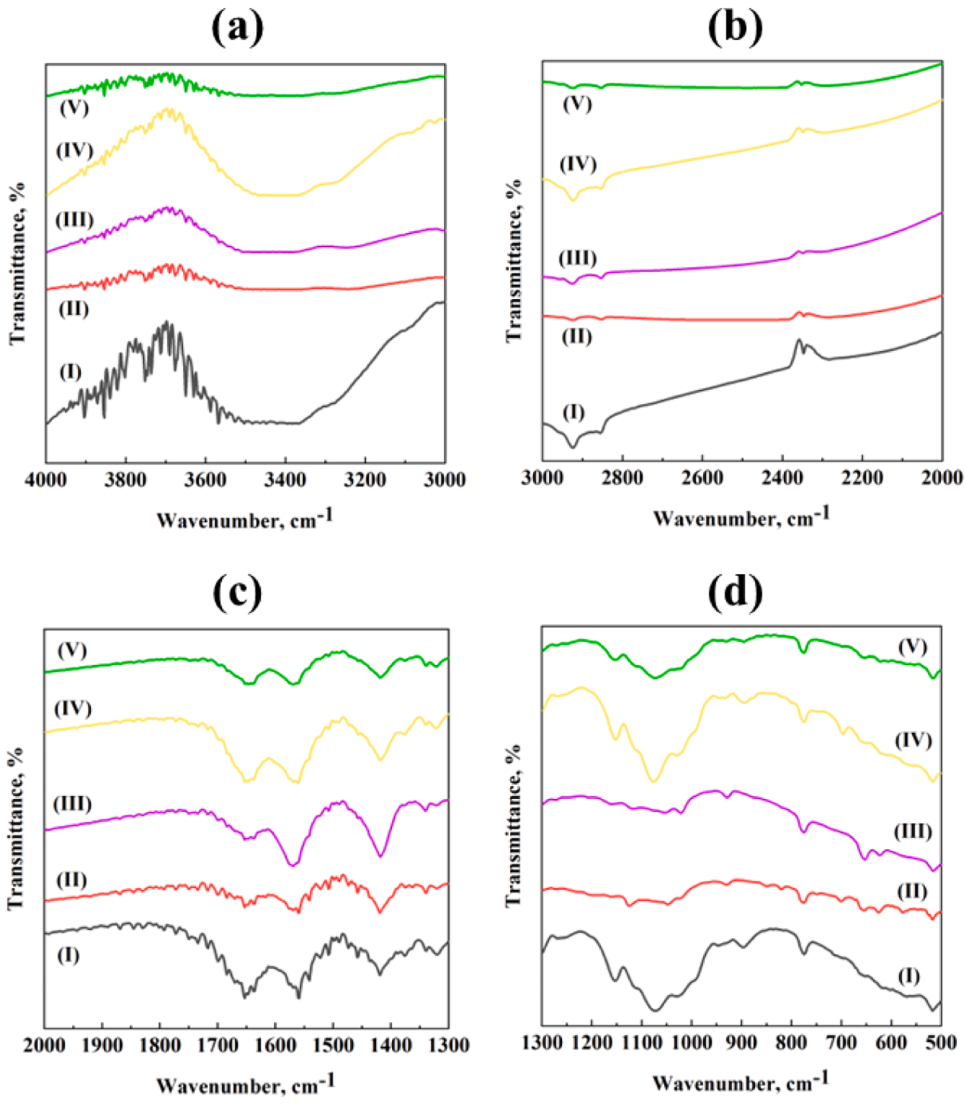

Fig. 9. FT-IR spectra enlargements of the regions: (a) 4000–3000 cm^{-1}; (b) 3000–2000 cm^{-1}; (c) 2000–1300 cm^{-1}; (d) 1300–500 cm^{-1}.

kinetic analysis are reported in Table 7.

For both MO and CV adsorption, the pseudo-first order model could not be applied reliably to the experimental data. Contrarily, the second-order kinetic model was much more effective in the description of the considered data: indeed, the calculated values of q_{eq} were virtually identical to the ones obtained experimentally, that is consistent with several data reported in the scientific literature [44]. From a physical perspective, the Blanchard model is reported to be describing accurately diffusion-limited phenomena, which could be the case of nanostructured adsorbents. Indeed, the differential form of this model depends on the square of the difference between q_{eq} and q(t): the deceleration rate of adsorption is amplified. The fact that mathematically this term is slowed down, could mean that adsorption is hindered by internal diffusion phenomena. Initially, when the difference between q_{eq} and q(t) reaches its maximum value, adsorption rate is amplified: adsorption takes place faster on the surface; secondly, when this "driving force" becomes smaller, adsorption rate is compromised due to internal diffusion [45].

Table 7
Kinetic parameters.

	Pseudo-first order			Pseudo-second order		
	q_{eq}, mg/g	k_1, min^{-1}	R^2	q_{eq}, mg/g	k_2, g (mg min)$^{-1}$	R^2
MO	9.94	2.9 E−5	0.26	1.70	0.066	0.999
CV	48.7	3.8 E−5	0.822	9.03	0.003	0.998

4. Conclusions

MO and CV adsorption was carried out using chitosan nano-structured adsorbents obtained by a supercritical fluid assisted drying. Collecting experimental datapoints at different initial concentrations and by FT-IR analysis, it was understood that CV adsorption is favored with respect to MO: CV was almost completely removed from the dye solutions using small amounts of adsorbents (50 mg), leading to large adsorption capacities. On the other hand, MO removal could be improved using fillers to intensify chemical interactions between the adsorbent and the dye itself.

The best-fitting adsorption isotherm was the Freundlich model for both dyes, meaning that adsorption was energetically non-homogenous. Kinetic analysis led to believe that the pseudo-second order model was more appropriate to describe the system dynamics; adsorption was limited by an internal diffusion step, coherently with the fact that the adsorbent was nanostructured.

In perspective, chitosan performance could be improved with respect to MO adsorption. It could be useful to check whether this system

behaves the same way for other anionic dyes, or there is a steric limitation regarding only methyl orange. As far as CV removal is concerned, chitosan is a highly performant adsorbent, and its uptake could be further explored and accelerated using composite nanostructured materials. Moreover, further studies will be carried out to investigate the effect of pH on adsorption, as well as desorption experiments and reusability.

CRediT authorship contribution statement

Alessandra Zanotti: Writing – original draft, Investigation. **Ernesto Reverchon:** Funding acquisition. **Stefano Cardea:** Writing – review & editing, Supervision. **Lucia Baldino:** Methodology, Data curation.

Declaration of Competing Interest

The authors declare that they have no known competing financial interests or personal relationships that could have appeared to influence the work reported in this paper.

Acknowledgements

The authors thank Alessandra Paolillo for her help provided during the development of the experiments, carried out during the development of her Master Thesis in Chemical Engineering at the Department of Industrial Engineering, University of Salerno.

Data availability

Data will be made available on request.

References

[1] A. Das, A. Dey, P-Nitrophenol -Bioremediation using potent Pseudomonas strain from the textile dye industry effluent, J. Environ. Chem. Eng. 8 (2020) 103830, https://doi.org/10.1016/j.jece.2020.103830.
[2] G. Mao, Y. Han, X. Liu, J. Crittenden, N. Huang, U.M. Ahmad, Technology status and trends of industrial wastewater treatment: A patent analysis, Chemosphere 288 (2022) 132483, https://doi.org/10.1016/j.chemosphere.2021.132483.
[3] A. Gholipour, H. Zahabi, A.I. Stefanakis, A novel pilot and full-scale constructed wetland study for glass industry wastewater treatment, Chemosphere 247 (2020) 125966, https://doi.org/10.1016/j.chemosphere.2020.125966.
[4] R. Gondi, S. Kavitha, R. Yukesh Kannah, O. Parthiba Karthikeyan, G. Kumar, V. Kumar Tyagi, J. Rajesh Banu, Algal-based system for removal of emerging pollutants from wastewater: A review, Bioresour. Technol. 344 (2022) 126245, https://doi.org/10.1016/j.biortech.2021.126245.
[5] V.K. Parida, D. Saidulu, A. Majumder, A. Srivastava, B. Gupta, A.K. Gupta, Emerging contaminants in wastewater: A critical review on occurrence, existing legislations, risk assessment, and sustainable treatment alternatives, J. Environ. Chem. Eng. 9 (2021) 105966, https://doi.org/10.1016/j.jece.2021.105966.
[6] E. Wanda, H. Nyoni, B. Mamba, T. Msagati, Occurrence of emerging micropollutants in water systems in Gauteng, Mpumalanga, and North West Provinces, South Africa, IJERPH 14 (2017) 79, https://doi.org/10.3390/ijerph14010079.
[7] N. Morin-Crini, E. Lichtfouse, M. Fourmentin, A.R.L. Ribeiro, C. Noutsopoulos, F. Mapelli, É. Fenyvesi, M.G.A. Vieira, L.A. Picos-Corrales, J.C. Moreno-Piraján, L. Giraldo, T. Sohajda, M.M. Huq, J. Soltan, G. Torri, M. Magureanu, C. Bradu, G. Crini, Removal of emerging contaminants from wastewater using advanced treatments. A review, Environ. Chem. Lett. 20 (2022) 1333–1375, https://doi.org/10.1007/s10311-021-01379-5.
[8] N.Z. Arman, S. Salmiati, A. Aris, M.R. Salim, T.H. Nazifa, M.S. Muhamad, M. Marpongahtun, A review on emerging pollutants in the water environment: existences, health effects and treatment processes, Water 13 (2021) 3258, https://doi.org/10.3390/w13223258.
[9] G. Crini, Non-conventional low-cost adsorbents for dye removal: A review, Bioresour. Technol. 97 (2006) 1061–1085, https://doi.org/10.1016/j.biortech.2005.05.001.
[10] R. Al-Tohamy, S.S. Ali, F. Li, K.M. Okasha, Y.A.-G. Mahmoud, T. Elsamahy, H. Jiao, Y. Fu, J. Sun, A critical review on the treatment of dye-containing wastewater: Ecotoxicological and health concerns of textile dyes and possible remediation approaches for environmental safety, Ecotoxicol. Environ. Saf. 231 (2022) 113160, https://doi.org/10.1016/j.ecoenv.2021.113160.
[11] M.A.M. Al-Alwani, N.A. Ludin, A.B. Mohamad, AbdA.H. Kadhum, A. Mukhlus, Application of dyes extracted from Alternanthera dentata leaves and Musa acuminata bracts as natural sensitizers for dye-sensitized solar cells, Spectrochim. Acta, Part A 192 (2018) 487–498, https://doi.org/10.1016/j.saa.2017.11.018.
[12] Md.A. Islam, I. Ali, S.M.A. Karim, Md.S. Hossain Firoz, A.-N. Chowdhury, D. W. Morton, M.J. Angove, Removal of dye from polluted water using novel nano manganese oxide-based materials, J. Water Process Eng. 32 (2019) 100911, https://doi.org/10.1016/j.jwpe.2019.100911.
[13] Q. Liu, Pollution and treatment of dye waste-water, IOP Conf. Ser.: Earth Environ. Sci. 514 (2020) 052001, https://doi.org/10.1088/1755-1315/514/5/052001.
[14] S. Varjani, P. Rakholiya, T. Shindhal, A.V. Shah, H.H. Ngo, Trends in dye industry effluent treatment and recovery of value added products, J. Water Process Eng. 39 (2021) 101734, https://doi.org/10.1016/j.jwpe.2020.101734.
[15] S. Benkhaya, S.M.' Rabet, A. El Harfi, A review on classifications, recent synthesis and applications of textile dyes, Inorg. Chem. Commun. 115 (2020) 107891, https://doi.org/10.1016/j.inoche.2020.107891.
[16] M.M. Hassan, C.M. Carr, Biomass-derived porous carbonaceous materials and their composites as adsorbents for cationic and anionic dyes: A review, Chemosphere 265 (2021) 129087, https://doi.org/10.1016/j.chemosphere.2020.129087.
[17] L.Y. Jun, L.S. Yon, N.M. Mubarak, C.H. Bing, S. Pan, M.K. Danquah, E.C. Abdullah, M. Khalid, An overview of immobilized enzyme technologies for dye and phenolic removal from wastewater, J. Environ. Chem. Eng. 7 (2019) 102961, https://doi.org/10.1016/j.jece.2019.102961.
[18] A. Saravanan, V.C. Deivayanai, P.S. Kumar, G. Rangasamy, R.V. Hemavathy, T. Harshana, N. Gayathri, K. Alagumalai, A detailed review on advanced oxidation process in treatment of wastewater: Mechanism, challenges and future outlook, Chemosphere 308 (2022) 136524, https://doi.org/10.1016/j.chemosphere.2022.136524.
[19] V. Katheresan, J. Kansedo, S.Y. Lau, Efficiency of various recent wastewater dye removal methods: A review, J. Environ. Chem. Eng. 6 (2018) 4676–4697, https://doi.org/10.1016/j.jece.2018.06.060.
[20] V. Golob, A. Vinder, M. Simonic, Efficiency of the coagulation/flocculation method for the treatment of dyebath effluents, Dyes Pigm. 67 (2005) 93–97, https://doi.org/10.1016/j.dyepig.2004.11.003.
[21] B. Shi, G. Li, D. Wang, C. Feng, H. Tang, Removal of direct dyes by coagulation: The performance of preformed polymeric aluminum species, J. Hazard. Mater. 143 (2007) 567–574, https://doi.org/10.1016/j.jhazmat.2006.09.076.
[22] M.T. Yagub, T.K. Sen, S. Afroze, H.M. Ang, Dye and its removal from aqueous solution by adsorption: A review, Adv. Colloid Interface Sci. 209 (2014) 172–184, https://doi.org/10.1016/j.cis.2014.04.002.
[23] B.S. Rathi, P.S. Kumar, Application of adsorption process for effective removal of emerging contaminants from water and wastewater, Environ. Pollut. 280 (2021) 116995, https://doi.org/10.1016/j.envpol.2021.116995.
[24] G. Neeraj, S. Krishnan, P. Senthil Kumar, K.R. Shriaishvarya, V. Vinoth Kumar, Performance study on sequestration of copper ions from contaminated water using newly synthesized high effective chitosan coated magnetic nanoparticles, J. Mol. Liq. 214 (2016) 335–346, https://doi.org/10.1016/j.molliq.2015.11.051.
[25] A. Saravanan, P.S. Kumar, A.A. Renita, Hybrid synthesis of novel material through acid modification followed ultrasonication to improve adsorption capacity for zinc removal, J. Clean. Prod. 172 (2018) 92–105, https://doi.org/10.1016/j.jclepro.2017.10.109.
[26] S. Kaur, G.S. Dhillon, The versatile biopolymer chitosan: potential sources, evaluation of extraction methods and applications, Crit. Rev. Microbiol. 40 (2014) 155–175, https://doi.org/10.3109/1040841X.2013.770385.
[27] C.P. Jiménez-Gómez, J.A. Cecilia, Chitosan: a natural biopolymer with a wide and varied range of applications, Molecules 25 (2020) 3981, https://doi.org/10.3390/molecules25173981.
[28] L. Baldino, S. Concilio, S. Cardea, I. De Marco, E. Reverchon, Complete glutaraldehyde elimination during chitosan hydrogel drying by SC-CO2 processing, J. Supercrit. Fluids 103 (2015) 70–76, https://doi.org/10.1016/j.supflu.2015.04.020.
[29] M. Guastaferro, L. Baldino, E. Reverchon, S. Cardea, Production of porous agarose-based structures: freeze-drying vs. supercritical CO2 drying, Gels 7 (2021) 198, https://doi.org/10.3390/gels7040198.
[30] A. Tabernero, L. Baldino, A. Misol, S. Cardea, E.M.M. Del Valle, Role of rheological properties on physical chitosan aerogels obtained by supercritical drying, Carbohydr. Polym. 233 (2020) 115850, https://doi.org/10.1016/j.carbpol.2020.115850.
[31] L. Zhai, Z. Bai, Y. Zhu, B. Wang, W. Luo, Fabrication of chitosan microspheres for efficient adsorption of methyl orange, Chin. J. Chem. Eng. 26 (2018) 657–666, https://doi.org/10.1016/j.cjche.2017.08.015.
[32] Y. Jiang, B. Liu, J. Xu, K. Pan, H. Hou, J. Hu, J. Yang, Cross-linked chitosan/β-cyclodextrin composite for selective removal of methyl orange: Adsorption performance and mechanism, Carbohydr. Polym. 182 (2018) 106–114, https://doi.org/10.1016/j.carbpol.2017.10.097.
[33] U. Habiba, T.A. Siddique, J.J. Li Lee, T.C. Joo, B.C. Ang, A.M. Afifi, Adsorption study of methyl orange by chitosan/polyvinyl alcohol/zeolite electrospun composite nanofibrous membrane, Carbohydr. Polym. 191 (2018) 79–85, https://doi.org/10.1016/j.carbpol.2018.02.081.
[34] S.H. Vithalkar, R.M. Jugade, Adsorptive removal of crystal violet from aqueous solution by cross-linked chitosan coated bentonite, Mater. Today.: Proc. 29 (2020) 1025–1032, https://doi.org/10.1016/j.matpr.2020.04.705.
[35] M. Massoudinejad, H. Rasoulzadeh, M. Ghaderpoori, Magnetic chitosan nanocomposite: Fabrication, properties, and optimization for adsorptive removal of crystal violet from aqueous solutions, Carbohydr. Polym. 206 (2019) 844–853, https://doi.org/10.1016/j.carbpol.2018.11.048.
[36] J. Qin, F. Qiu, X. Rong, J. Yan, H. Zhao, D. Yang, Adsorption behavior of crystal violet from aqueous solutions with chitosan–graphite oxide modified polyurethane as an adsorbent, J. Appl. Polym. Sci. 132 (2015) app.41828, https://doi.org/10.1002/app.41828.

[37] A.S.K. Kumar, S.-J. Jiang, Chitosan-functionalized graphene oxide: A novel adsorbent an efficient adsorption of arsenic from aqueous solution, J. Environ. Chem. Eng. 4 (2016) 1698–1713, https://doi.org/10.1016/j.jece.2016.02.035.
[38] M. Benjelloun, Y. Miyah, G. Akdemir Evrendilek, F. Zerrouq, S. Lairini, Recent advances in adsorption kinetic models: their application to dye types, Arab. J. Chem. 14 (2021) 103031, https://doi.org/10.1016/j.arabjc.2021.103031.
[39] E.D. Revellame, D.L. Fortela, W. Sharp, R. Hernandez, M.E. Zappi, Adsorption kinetic modeling using pseudo-first order and pseudo-second order rate laws: A review, Clean. Eng. Technol. 1 (2020) 100032, https://doi.org/10.1016/j.clet.2020.100032.
[40] W.S. Wan Ngah, L.C. Teong, R.H. Toh, M.A.K.M. Hanafiah, Comparative study on adsorption and desorption of Cu(II) ions by three types of chitosan–zeolite composites, Chem. Eng. J. 223 (2013) 231–238, https://doi.org/10.1016/j.cej.2013.02.090.
[41] M. Yazdani, E. Virolainen, K. Conley, R. Vahala, Chitosan–Zinc(II) complexes as a bio-sorbent for the adsorptive abatement of phosphate: mechanism of complexation and assessment of adsorption performance, Polymers 10 (2017) 25, https://doi.org/10.3390/polym10010025.
[42] V. Sabna, S.G. Thampi, S. Chandrakaran, Adsorption of crystal violet onto functionalised multi-walled carbon nanotubes: Equilibrium and kinetic studies, Ecotoxicol. Environ. Saf. 134 (2016) 390–397, https://doi.org/10.1016/j.ecoenv.2015.09.018.
[43] L. Ayed, E. Khelifi, H.B. Jannet, H. Miladi, A. Cheref, S. Achour, A. Bakhrouf, Response surface methodology for decolorization of azo dye Methyl Orange by bacterial consortium: Produced enzymes and metabolites characterization, Chem. Eng. J. 165 (2010) 200–208, https://doi.org/10.1016/j.cej.2010.09.018.
[44] H. Moussout, H. Ahlafi, M. Aazza, H. Maghat, Critical of linear and nonlinear equations of pseudo-first order and pseudo-second order kinetic models, Karbala Int. J. Mod. Sci. 4 (2018) 244–254, https://doi.org/10.1016/j.kijoms.2018.04.001.
[45] M.A. Hubbe, S. Azizian, S. Douven, Implications of apparent pseudo-second-order adsorption kinetics onto cellulosic materials: a review, Bioresources 14 (2019) 7582–7626.